Supporting Information

A gradient poly(vinyl alcohol)/polysaccharide composite film towards robust and fast stimuli-responsive actuators by interface co-precipitation

Bai Huang [a,b], Ge Zhu [b], Shuzhan Wang [a], Qunyang Li [a], Jérémie Viguié [b], Hui He [a,*], and Alain Dufresne [b,*]

[a] School of Materials Science and Engineering, South China University of Technology, Wushan Road, Tianhe District, Guangzhou, Guangdong, 510640, P. R. China

[b] Univ. Grenoble Alpes, CNRS, Grenoble INP, LGP2, F-38000 Grenoble, France

*Corresponding authors:

(Hui HE) E-mail: pshuihe@scut.edu.cn.

(Alain DUFRESNE) E-mail: alain.dufresne@pagora.grenoble-inp.fr.

Contents

1. Supporting Data (Table S1-S3 and Figure S1-S3)

Table S1. Water-induced deformation performance of PVA composite films

Sample	Curvature (mm^{-1})	Time (s)	Speed ($mm^{-1} \cdot s^{-1}$)
PVA/CS-CNF0	-	-	-
PVA/CS-CNF5	0.52±0.06	52±7	0.0303±0.0048
PVA/CS-CNF10	0.57±0.07	64±9	0.0352±0.0043
PVA/CS-CNF15	0.69±0.05	67±5	0.0392±0.0070
PVA/CS-CNF20	0.55±0.05	161±9	0.0168±0.0031
PVA/CS-CNF30	0.53±0.06	241±11	0.0106±0.0028
PVA/CS-CNF40	0.52±0.06	306±7	0.0085±0.0014

Table S2. Data collection pertaining to Figure 2f

Material	Curvature (mm^{-1})	Time (s)	Conditions	Reference
PNIPAAm/ALG	0.62	3600	T=42 °C	19a [1]
Silk Fibroin Film	0.62	0.4	T=20 °C	19b [2]
PDMS/PEDOT:PSS	0.42	140	T=20 °C	19c [3]
Pollen paper	0.19	80	T=20 °C	7a [4]
PLLA Films	0.6	5	T=75 °C	19d [5]
Graphene hydrogels	0.14	200	T=20 °C	14 [6]
NFC nanopapers	0.193	35	T=20 °C	19e [7]
EVOH/CNC	0.314	1.2	T=30 °C	19f [8]
PVA/PET film	0.09	700	T=20 °C	19g [9]
PI/CNF	0.65	6	T=85 °C	19h [10]
GO/PPy bilayer	0.41	10	T=20 °C	1c [11]
Polyester paper	0.175	600	T=20 °C	19i [12]
LDPE/PVC	0.25	40	T=20 °C	1b [13]
CS/cellulose	0.14	180	T=20 °C	15b [14]
PA6/CNC/PEGDA	0.09	8	T=20 °C	19j [15]
PVA/CS/CNF	**0.69**	**67**	**T=20 °C**	**This work**

Table S3. Mechanical propertie for PVA/polysaccharide composite films

Sample	Tensile strength (MPa)	Young's modulus (MPa)	Elongation at break (%)	Toughness* ($MJ \cdot m^{-3}$)
PVA/CS-CNF0	57.1±5.7	2090±130	13.6±8.1	5.7±2.4
PVA/CS-CNF5	58.1±3.4	1910±120	44.6±8.9	21.6±4.7
PVA/CS-CNF10	62.4±2.6	1790±130	49.6±6.1	24.7±3.5
PVA/CS-CNF15	63.6±6.9	1710±60	51.3±11.4	26.9±4.5
PVA/CS-CNF20	57.9±3.2	1400±140	56.7±9.2	22.7±3.7
PVA/CS-CNF30	46.8±3.1	750±80	54.5±4.1	21.1±1.3
PVA/CS-CNF40	44.1±2.3	700±160	54.1±3.9	17.1±3.0

* Toughness (T) is defined as the area surrounded by the stress-strain (σ-ε) curves as following [16, 17]:

$$T = \int_0^{\varepsilon_{max}} \sigma \cdot d\varepsilon$$

where σ and ε represent stress (MPa) and strain ($mm \cdot mm^{-1}$), respectively.

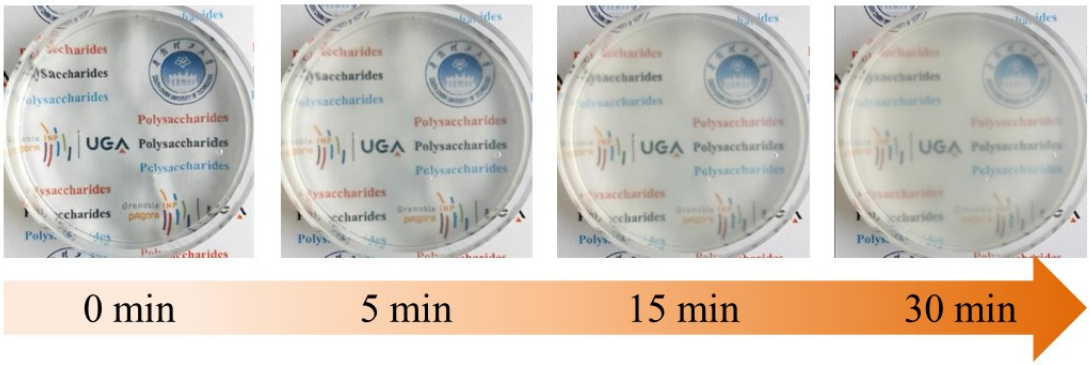

Figure S1. The formation process of the deposited layer.

The picture shows the change after casting CNF suspension on top of PVA/CS solution. At the beginning, the system was transparent, and the text in the background could be clearly seen. As the deposition time increases, the system becomes white, which is caused by the formation of a white deposition layer.

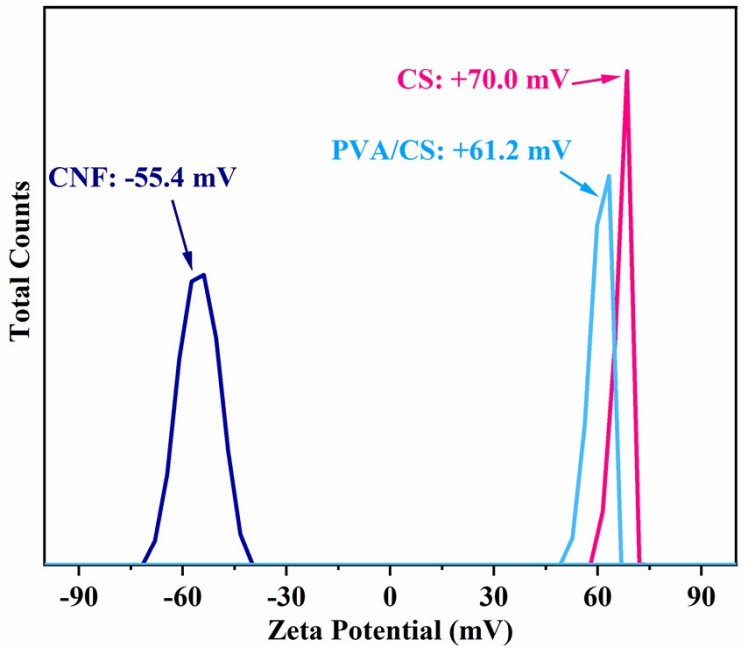

Figure S2. Zeta potential for CNF suspension, CS solution and PVA/CS solution.

It can be seen from the figure that carboxylated CNF has a significant negative charge (-55.4 mV), while the potential of chitosan (CS) is positive (+70.0 mV). The huge potential difference lays the foundation for the implementation of interface co-precipitation and the performance improvement of composite films.

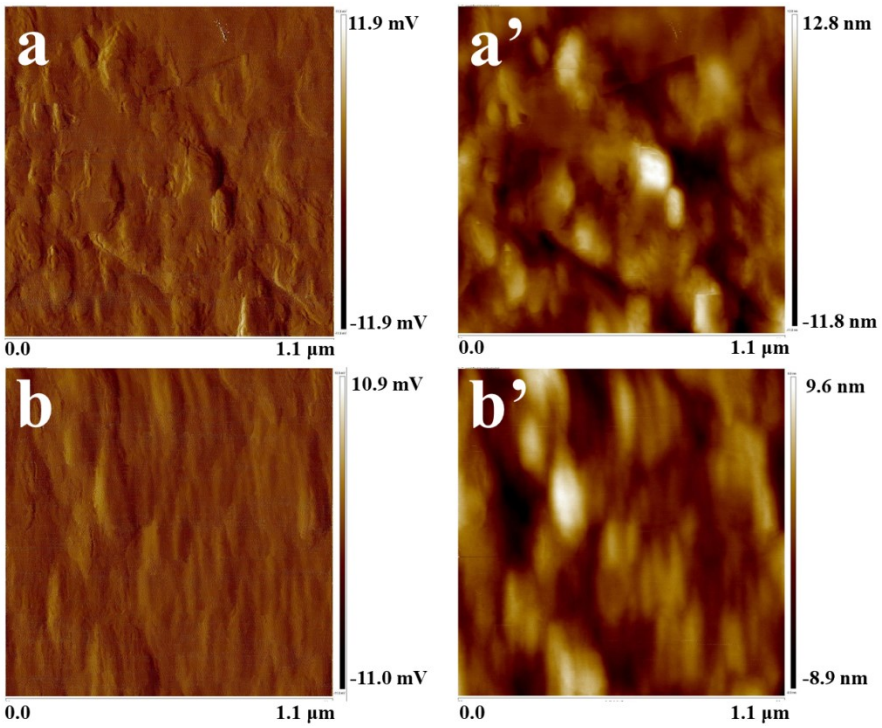

Figure S3. AFM images of the surface for PVA/CS-CNF0 (a, a') and PVA/CS-CNF15 (b, b').

It can be seen that the surface of the PVA/CS-CNF15 sample exhibits obvious alignment stripes, which are caused by the shrinkage of deposited layer during the drying process. So that the CNF embedded in the deposited layer obtains a certain orientation arrangement.

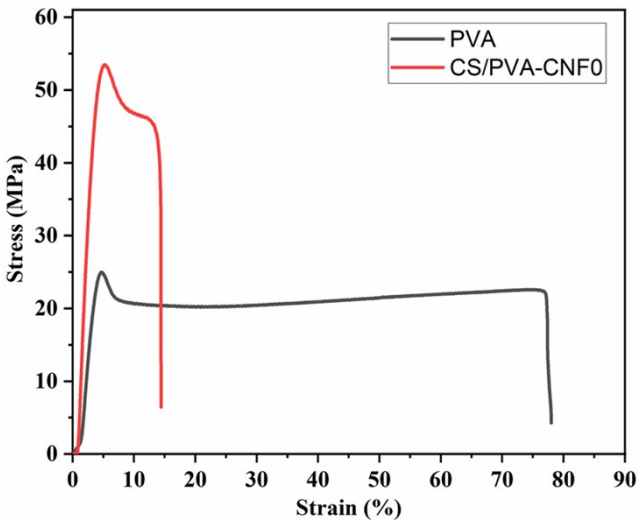

Figure S4. Typical stress-strain curve of PVA composite film after adding chitosan.

The addition of 50 wt.% chitosan significantly increased the tensile strength of the PVA composite film, but also significantly reduced the elongation at break.

2. Supplementary Information Movies

Movie S1. Interface co-precipitation process: Formation of deposited layer.

Movie S2. Water-induced deformation behavior of samples deposited at different time (0 min, 10 min, 15 min).

Movie S3. Deformation of the samples with different cutting directions in water.

Movie S4. Deformation of PVA/CS-CNF15 at pH = 4.

Movie S5. Deformation of PVA/CS-CNF15 between water and 3M NaCl solution.

Movie S6. Deformation and simulation of *Confederate Jasmine* with composite films.

.

3. References

[1]D. Podstawczyk, M. Nizioł, P. Szymczyk‐Ziółkowska, et al. Development of Thermoinks for 4D Direct Printing of Temperature‐Induced Self‐Rolling Hydrogel Actuators[J]. Adv. Funct. Mater.,2021,31(15):2009664.

[2]G. Manikandan, A. Murali, R. Kumar, et al. Rapid Moisture-Responsive Silk Fibroin Actuators[J]. ACS Appl. Mater. Interfaces,2021,13(7):8880-8888.

[3]C. Dingler, H. Muller, M. Wieland, et al. From Understanding Mechanical Behavior to Curvature Prediction of Humidity-Triggered Bilayer Actuators[J]. Adv. Mater.,2021,33(9):2007982.

[4]Z. Zhao, Y. Hwang, Y. Yang, et al. Actuation and locomotion driven by moisture in paper made with natural pollen[J]. Proc. Natl. Acad. Sci. U. S. A.,2020,117(16):8711-8718.

[5]W. Peng, G. Zhang, J. Liu, et al. Light‐Coded Digital Crystallinity Patterns Toward Bioinspired 4D Transformation of Shape‐Memory Polymers[J]. Adv. Funct. Mater.,2020,30(19):2000522.

[6]A. López‐Díaz, A. Martín‐Pacheco, A. M. Rodríguez, et al. Concentration Gradient‐Based Soft Robotics: Hydrogels Out of Water[J]. Adv. Funct. Mater.,2020,30(46):2004417.

[7]M. Chemin, B. Beaumal, B. Cathala, et al. pH-Responsive Properties of Asymmetric Nanopapers of Nanofibrillated Cellulose[J]. Nanomaterials (Basel),2020,10(7):1380.

[8]Q. Zhu, Y. Jin, W. Wang, et al. Bioinspired Smart Moisture Actuators Based on Nanoscale Cellulose Materials and Porous, Hydrophilic EVOH Nanofibrous

Membranes[J]. ACS Appl. Mater. Interfaces,2019,11(1):1440-1448.

[9]C. Xu, B. Ma, S. Yuan, et al. High‐Resolution Patterning of Liquid Metal on Hydrogel for Flexible, Stretchable, and Self‐Healing Electronics[J]. Adv. Electron. Mater.,2019,6(1):1900721.

[10]Y. Kuang, C. Chen, J. Cheng, et al. Selectively aligned cellulose nanofibers towards high-performance soft actuators[J]. Extreme Mech. Lett.,2019,29:100463.

[11]Y. Dong, J. Wang, X. Guo, et al. Multi-stimuli-responsive programmable biomimetic actuator[J]. Nat. Commun.,2019,10(1):4087.

[12]W. Wang, C. Li, M. Cho, et al. Soft Tendril-Inspired Grippers: Shape Morphing of Programmable Polymer-Paper Bilayer Composites[J]. ACS Appl. Mater. Interfaces,2018,10(12):10419-10427.

[13]H. Kim, H. Lee, I. Ha, et al. Biomimetic Color Changing Anisotropic Soft Actuators with Integrated Metal Nanowire Percolation Network Transparent Heaters for Soft Robotics[J]. Adv. Funct. Mater.,2018,28(32):1801847.

[14]J. Duan, X. Liang, K. Zhu, et al. Bilayer hydrogel actuators with tight interfacial adhesion fully constructed from natural polysaccharides[J]. Soft Matter,2017,13(2):345-354.

[15]T. Wu, J. Li, J. Li, et al. A bio-inspired cellulose nanocrystal-based nanocomposite photonic film with hyper-reflection and humidity-responsive actuator properties[J]. J. Mater. Chem. C,2016,4(41):9687-9696.

[16]C. Jiao, J. Zhang, T. Liu, et al. Mechanically Strong, Tough, and Shape Deformable Poly(acrylamide-co-vinylimidazole) Hydrogels Based on Cu(2+) Complexation[J].

ACS Appl Mater Interfaces,2020,12(39):44205-44214.

[17]P. Yu, H. He, Y. Luo, et al. Reinforcement of Natural Rubber: The Use of in Situ Regenerated Cellulose from Alkaline–Urea–Aqueous System[J]. Macromolecules,2017,50(18):7211-7221.